Magnesium Promotes Structural Integrity and Conformational Switching Action of a Calcium Sensor Protein†

Sulakshana Mukherjee, P. M. Krishna Mohan, and Kandala V. R. Chary*

Department of Chemical Sciences, Tata Institute of Fundamental Research, Homi Bhabha Road, Mumbai 400 005, India

Received October 12, 2006; Revised Manuscript Received December 23, 2006

ABSTRACT: Calcium binding proteins carry out various signal transduction processes upon binding to Ca^{2+}. In general, these proteins perform their functions in a high background of Mg^{2+}. Here, we report the role of Mg^{2+} on a calcium sensor protein from *Entamoeba histolytica* (*Eh*CaBP), containing four Ca^{2+}-binding sites. Mg^{2+}-bound *Eh*CaBP exists as a monomer with a conformation different from that of the holo- and apo-*Eh*CaBP. NMR and biophysical data on *Eh*CaBP demonstrate that Mg^{2+} stabilizes the closed conformation of the apo form. In the presence of Mg^{2+}, the partially collapsed apo-*Eh*CaBP gains stability and structural integrity. Mg^{2+} binds to only 3 out of 4 calcium binding sites in *Eh*CaBP. The Ca^{2+} binding affinity and cooperativity of the conformational switching from the "closed" to the "open" state is significantly modulated by the presence of Mg^{2+}. This fine-tuning of the Ca^{2+} concentration to switch its conformation is essential for CaBPs to carry out the signal transduction process efficiently.

Calcium plays a vital role in cellular signal transduction. The signaling is carried out by ATP-driven Ca^{2+} pumps, ion channels, and calcium binding proteins (CaBPs). The signaling by CaBPs is carried out during the transient cytosolic increase in Ca^{2+} concentration which varies from nM (in the resting cell) to μM range (stimulated cell) (*1*). The mechanism of interaction of Ca^{2+} with CaBPs helps in understanding the signal transduction within a cell. CaBPs usually bind Ca^{2+} via well-known EF-hand motif (*2*), also known as the helix−loop−helix motif. EF-hand CaBPs (EF-CaBP) can be broadly classified into two subgroups, which are identified as Ca^{2+} dependent regulatory proteins (such as calmodulin (CaM) and troponin-C (TnC)) and as cytosolic buffers (such as D_{9k}-calbindin) (*3*, *4*). The proteins belonging to the first group undergo major conformational change upon Ca^{2+} binding (*3*−*8*), exposing hydrophobic surface to interact with target proteins. As far as the second group is concerned, the conformational changes upon Ca^{2+} binding are more modest compared to those observed in Ca^{2+} sensor class.

In living cells, all the essential activities of the EF-CaBPs are carried out in the background of 100−10000 folds of higher cytosolic Mg^{2+} concentration compared to Ca^{2+} (*1*). Hence, to gain information about the EF-CaBPs under physiological conditions it is important to study Ca^{2+} interaction with EF-CaBPs in the presence of large Mg^{2+} concentration. The dehydration energy for Mg^{2+} (−436 kcal mol^{-1}) is higher than that of Ca^{2+} (−358 kcal mol^{-1}) due to the former's higher charge density. For the same reason, Mg^{2+} has a 10^3 times slower desolvation rate than Ca^{2+} (*9*). The EF-hand binds to Ca^{2+} (ionic radius 1.00 Å) in pentagonal bipyramidal geometry with a coordination number of seven while in binding to Mg^{2+} (ionic radius 0.72 Å) an octahedral geometry with a coordination number of six is preferred due to its smaller ionic size (*9*). Ca^{2+}−ligand bond distances are typically 2.3-2.6 Å, whereas Mg^{2+}−ligand bond length are relatively shorter (2.0-2.1 Å) (*10*).

In EF-CaBPs, the Ca^{2+} binding loop is a highly conserved single stretch of twelve amino acid residues (Scheme 1). The Glu residue at the +12th position plays a vital role in Ca^{2+}/Mg^{2+} selectivity (*11*). This residue uses both the side-chain carboxyl oxygens in its coordination with Ca^{2+} and forms a bidentate ligand. E12D mutation is known to destabilize the pentagonal bipyramidal geometry of the Ca^{2+} binding site (*12*). The Asp with its relatively shorter side chain, however, participates in Ca^{2+} coordination as a monodentate ligand. This results in an octahedral geometry at the metal binding site and facilitates Mg^{2+} binding even more strongly than Ca^{2+} (*13*, *14*). Recently several CaBPs have been shown to adopt a partially collapsed or molten globular like structure in their Ca^{2+}-free form (*14*−*17*), and Mg^{2+} is shown to stabilize these proteins in their Ca^{2+}-free form (*14*−*16*, *18*). However, the mechanism by which such stabilization is achieved is not very clear. In the present study, we have attempted to address the role of Mg^{2+} in the stabilization of an EF-CaBP from *Entamoeba histolytica* (*Eh*CaBP[1]), which belongs to the calcium sensor family. The protein has a well folded structure in its holo state (PDB ID: 1JFK) (*19*) but a partially collapsed structure in its apo state (*17*). It is a 134 amino acid residue ($M^r \sim 14.9$ kDa) monomeric protein

† The facilities provided by the National Facility for High Field NMR, at TIFR, supported by DST, DBT, CSIR, and TIFR, are gratefully acknowledged. S.M. and P.M.K.M. are recipients of the TIFR Alumni Association Scholarship (2003−2005) for career development, supported by the TIFR endowment fund.

* Corresponding author.: Tel: 91 22 22782489. Fax: 91 22 2280 4610. E-mail: chary@tifr.res.in.

[1] Abbreviations: NMR, nuclear magnetic resonance; ITC, isothermal calorimetry; HSQC, heteronuclear single quantum coherence; EhCaBP, *Entamoeba histolytica* calcium binding protein; CaM, calmodulin; TnC, troponin C; EGTA, ethyleneglycol bis (beta-aminoethyl ether)- *N*,*N*′-tetraacetate; ANS, 8-anilino-1-naphthalene sulfonic acid; DLS, dynamic light scattering.

10.1021/bi0621260 CCC: $37.00
Published on Web 02/22/2007

Scheme 1

1	2	3	4	5	6	7	8	9	10	11	12
D	.	(D/N)	.	(D/N)	G	.	.	.	.	.	E
X		Y		Z		-Y		-X			-Z

containing four canonical EF-hand Ca^{2+}-binding loops. Calcium is thought to be involved in the pathogenic mechanisms of amoebiasis and the mechanisms governing pathogenesis. The structural topology of *Eh*CaBP resembles that of CaM and TnC. *Eh*CaBP basically consists of two globular domains connected by a flexible 8 amino acid residue linker. The present study provides a rationale for the fine conformational tuning of the calcium sensor protein in the presence of Mg^{2+} in order to carry out various signal transduction processes.

MATERIALS AND METHODS

Protein Expression and Purification. The protocol used for overexpression and purification of *Eh*CaBP in its Ca^{2+}-bound and Ca^{2+}-free forms is as described earlier (*17*, *19*, *20*).

Gel Permeation. Protein samples (300 μL of 39 μM) in 50 mM Tris·HCl buffer, 100 mM NaCl, pH 7.4, in the presence of 0.5 mM EGTA (apo-*Eh*CaBP) and 10 mM Ca^{2+} (holo-*Eh*CaBP), 30 mM Mg^{2+} (apo-*Eh*CaBP), were loaded on a Superdex G-75 gel permeation column (120 mL bed volume), equilibrated in the same buffer and connected to the low-pressure liquid chromatography system (Biorad). The flow rate for the experiment was 0.3 mL/min. Apparent molecular masses were calculated as described earlier (*17*).

Circular Dichroism. Thermal stability was determined by monitoring the molar ellipticity at 222 nm as a function of temperature, at 1 °C intervals, on a JASCO J-810 spectropolarimeter equipped with Peltier controlled temperature controller and 0.1 cm path length cuvettes. Protein concentration was 36 μM (50 mM Tris·HCl buffer, 90 mM NaCl in the case of apo-*Eh*CaBP and holo-*Eh*CaBP, 30 mM $MgCl_2$ in the case of Mg-*Eh*CaBP) at pH 7.4.

The stabilities of all the three forms were also studied against chemical denaturants like GdmCl. 10 μM protein samples were used for holo, apo, and Mg-bound forms of *Eh*CaBP (50 mM Tris·HCl buffer, 90 mM NaCl in the case of apo-*Eh*CaBP and holo-*Eh*CaBP, 30 mM $MgCl_2$ in the case of Mg-*Eh*CaBP) at pH 7.4. The GdmCl induced unfolding of *Eh*CaBP was analyzed and fitted to the linear extrapolation model with an assumption of two-state unfolding (*21*). The baselines before (Y_N) and after (Y_U) the actual unfolding were assumed to be straight lines, where k_N and k_U are the slopes, b_N and b_U are intercepts, and [D] is the denaturant concentration. The free energy toward unfolding by GdmCl, ΔG_{NU}, is assumed to obey the linear equation

$$\Delta G_{NU} = \Delta G_{NU}(H_2O) - m_D[D] \quad (1)$$

The GdmCl concentration at the transition midpoint (C_m) was calculated from eq 1 by setting ΔG_{NU} to zero. The errors in the reported values of the different parameters were estimated to one standard deviation. The standard deviations were obtained directly from the fitting procedures. The data were normalized according to

$$F_{app} = \frac{(Y_O - Y_N)}{(Y_U - Y_N)} \quad (2)$$

Y_N and Y_U hence correspond to the ellipticity of the native and the unfolded state, respectively, as a function of GdmCl concentration and fitted to

$$F_{app} = \frac{e^{-(\Delta G_{NU}(H_2O) - m_D[D])/RT}}{1 + e^{-(\Delta G_{NU}(H_2O) - m_D[D])/RT}} \quad (3)$$

where $\Delta G_{NU}(H_2O)$ is the unfolding free energy in pure water, m_D is the influence of denaturant concentration on the stability, R is the molar gas constant, and T is the absolute temperature.

Fluorescence Spectroscopy. The 8-anilino-1-naphthalene sulfonic acid (ANS)-binding experiments were performed on a spectrofluorimeter (SPEX Fluorolog) at 25 °C using 1 mL of 10.35 μM of apo-*Eh*CaBP in 50 mM Tris and 100 mM NaCl with excitation and emission slits of 0.7 nm. The ANS fluorescence emission spectra were recorded between 400 and 600 nm with excitation at 389 nm. The protein was saturated with 115 μM ANS. Two different Ca^{2+} titrations were carried out, one in the presence of 90 mM NaCl and the second in the presence of 30 mM $MgCl_2$. Ca^{2+} was successively added to the ANS containing protein solution, by taking 1 μL aliquots of $CaCl_2$, from a 1 mM stock solution, and the fluorescence emission was recorded. Spectra were corrected for ANS fluorescence in buffer without the protein. The normalized intensity at 476 nm (Y) was fitted to the Hill equation (eq 4),

$$Y = \frac{[Ca^{2+}]^n}{[Ca^{2+}] + K_d} \quad (4)$$

where $[Ca^{2+}]$ is the free Ca^{2+} concentration, K_d is the apparent dissociation constant, and n denotes the Hill coefficient.

Isothermal Calorimetry. ITC measurements were performed with a Microcal Omega titration calorimeter at 298 K. Samples were centrifuged and degassed prior to the titration. A typical titration consisted of injecting 3 μL aliquots of 10 mM Ca^{2+} solution (diluted from 1 M standard $CaCl_2$ solution supplied from Sigma-Aldrich chemicals) into 145 μM protein solution (1.4 mL) after every 3 min to ensure that the titration peak returned to the baseline prior to the next injection. A total of 45 injections were carried out. Aliquots of concentrated ligand solution were injected into the buffer solution (without the protein) in a separate ITC run, to subtract the heat of dilution. Two sets of titrations were carried out, (i) apo-*Eh*CaBP in 50 mM Tris (pH 7.0) and 90 mM NaCl and (ii) apo-*Eh*CaBP in 50 mM Tris (pH 7.0) and 30 mM $MgCl_2$. Mg^{2+} titration was carried out using 850 μM of apo protein (stock concentration of Mg^{2+} used 100 mM) in 50 mM Tris (pH 7.4) and 90 mM NaCl. The ITC data were analyzed using the software ORIGIN (supplied with Omega Microcalorimeter). The amount of heat released per addition of the titrant was fitted to four sequential binding sites on the protein as given by Wisemen et al. (*22*).

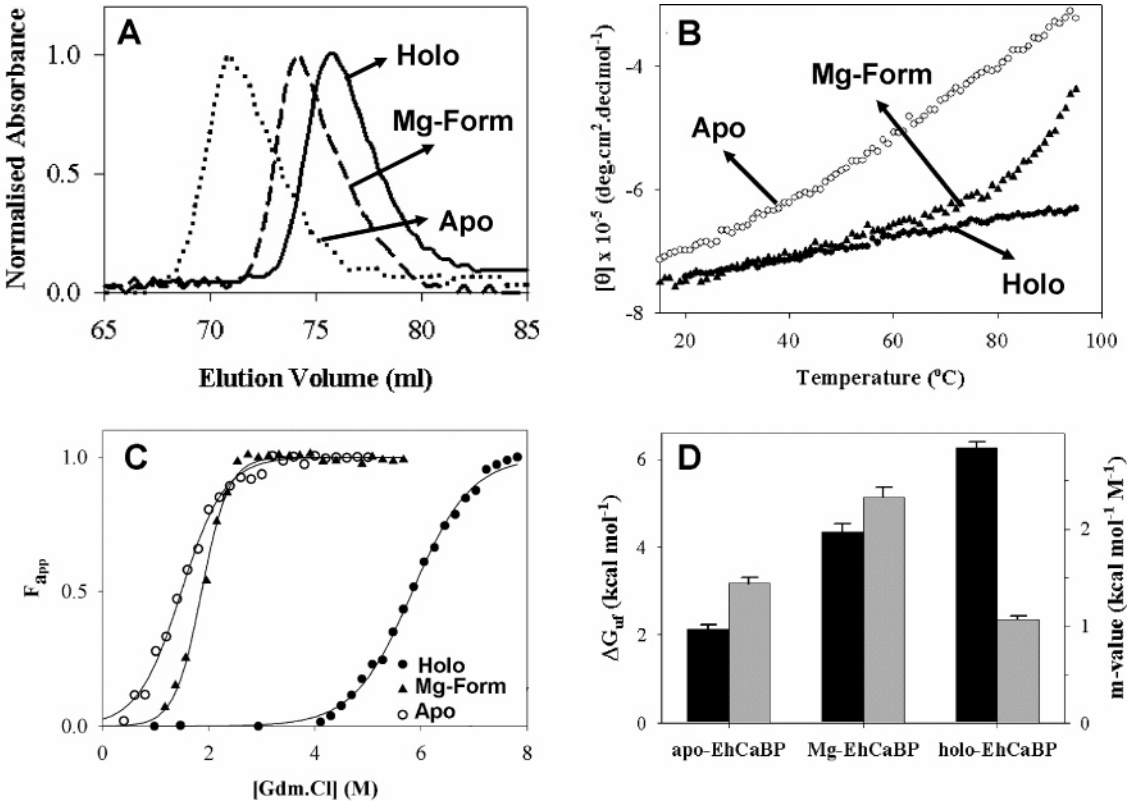

FIGURE 1: (A) Gel filtration elution profiles of apo-, holo-, and Mg-*Eh*CaBP. (B) Thermal denaturation in the range 15−95 °C, at an interval of 1 °C. (C) GdmCl denaturation (at 25 °C) of apo-, Mg-, and holo-*Eh*CaBP as monitored by CD at 222 nm. (D) Histogram showing the ΔG (shown in black) and m values (shown in gray) for the three different forms of *Eh*CaBP.

NMR Spectroscopy. NMR experiments were carried out on a Varian Inova 600 MHz NMR spectrometer equipped with a pulsed field gradient unit and triple resonance probe with actively shielded Z-gradient, operating at a ^{1}H frequency of 599.862 MHz. Sensitivity enhanced 2D [^{15}N−^{1}H] heteronuclear single quantum correlation (HSQC) (*23*) spectra of the protein sample (pH 7.4 and temperature = 25 °C) were recorded with the ^{1}H carrier placed on H_2O resonance (4.78 ppm) and ^{15}N carrier at 123.8 ppm. Spectra were processed using the VNMR 6.1B (Varian) and Felix 2002 (Molecular Simulations Inc.). The 2D [^{15}N−^{1}H] HSQC data were zero filled 2-fold along the t_1 dimension and apodized using $\pi/3$ shifted sine-square-bell window functions along both the dimensions prior to 2D Fourier transformation. Integral volumes for the individual ^{15}N−^{1}H cross peaks in the resultant spectra were measured using Felix 2002.

Hydrogen exchange experiments were carried out on Mg-*Eh*CaBP as described earlier (*17*) with time intervals of 45, 450, 900, 1800, 3300, 5400, 14508, and 15556 s between the ^2H_2O pulse and the Ca^{2+} pulse.

Ca^{2+} titration was carried out with standard 100 mM $CaCl_2$ (Fluka). The protein concentration was 1.2 mM in 50 mM Tris (pH = 7.4), 90 mM ionic strength (90 mM NaCl and 30 mM $MgCl_2$ in the presence and in the absence of Mg^{2+}, respectively). For each titration, an aliquot of 1 μL of the stock solution was added to the NMR tube containing the protein solution, mixed and followed by recording 2D [^{15}N−^{1}H] HSQC at 25 °C. The total experimental time for each spectrum was 20 min, and the total volume added was 30 μL. HSQC spectra were processed with identical processing parameters.

Mn^{2+} titration was carried out with the holo-*Eh*CaBP. A stock solution of 10 mM $MnCl_2$ was used for this purpose. Excess of Ca^{2+} in the protein sample was removed using a 3 kDa cutoff Amicon centricon unit, by washing protein solution six times with NMR buffer (50 mM Tris + 0.1 M NaCl + 30 mM $MgCl_2$) containing 10% ^2H_2O and pH 7.4. To maintain Ca^{2+} concentration below saturation ~0.5 mM EGTA was added to the final protein. Estimated protein concentration was 0.9 mM. Titrations were performed at 25 °C with 0.55 mL of protein samples (pH 7.4) in a mixed solvent of 90% H_2O and 10% ^2H_2O. No further titration was carried out when the water line-shape started showing up broadening due to the paramagnetic Mn^{2+}.

RESULTS

Mg-EhCaBP Exists as Monomer. Figure 1A shows the gel filtration elution profiles of holo-, apo-, and Mg-*Eh*CaBP. The elution volume is distinctly different in the case of Mg-*Eh*CaBP from those of the apo and holo forms of the protein. The apparent molecular mass of Mg-*Eh*CaBP thus calculated is 18.2 ± 0.1 kDa. The theoretical relative molecular mass of *Eh*CaBP is 14.9 kDa. The molecular mass obtained for Mg-*Eh*CaBP is in between the molecular masses for holo-*Eh*CaBP (16.8 ± 0.1 kDa) and apo-*Eh*CaBP (21.7 ± 0.1 kDa), which were reported earlier (*17*). The present data clearly suggest that Mg-*Eh*CaBP exists as a monomer. Thus the differences in the elution volume of Mg-*Eh*CaBP from that of the apo and holo forms clearly suggest that Mg-*Eh*CaBP adopts a conformation which is different from that of holo and apo forms of the protein (*24*). To rule out any possibility of formation of higher oligomers, we have carried out dynamic light scattering (DLS) experiments with all the

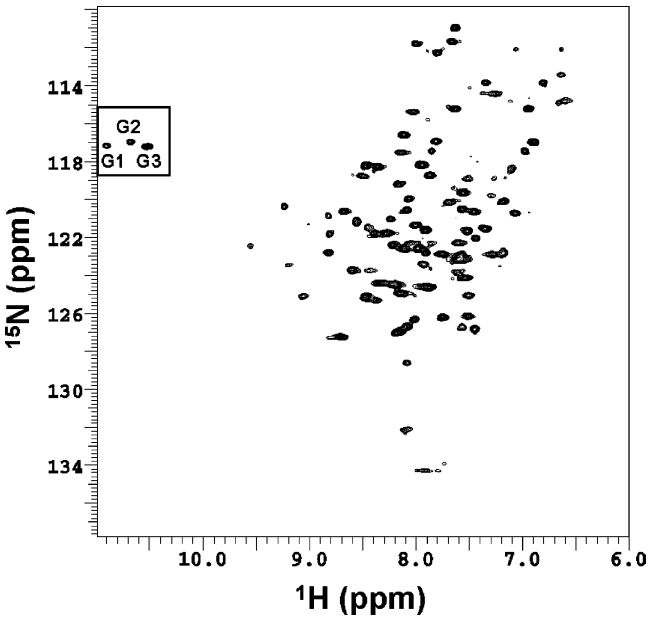

FIGURE 2: 2D [^{15}N−^{1}H] HSQC of Mg-*Eh*CaBP. Square box identifies the peaks belonging to the glycines at the 6th position (G-6) of the EF-hands labeled as G1, G2, and G3.

three forms at NMR sample concentrations (data not shown). Both DLS and gel permeation chromatography data reveal that the protein exists as a monomer in all the three forms even at concentrations as high as 1.2 mM.

Thermal and Chemical Denaturation of EhCaBP. Thermal unfolding monitored by CD reveals relatively higher stability for the Mg-*Eh*CaBP as compared to apo-*Eh*CaBP (Figure 1B). Holo-*Eh*CaBP on the other hand is found to be the most stable form and did not show any significant unfolding even at temperatures as high as 95 °C. The unfolding transition of the apo-*Eh*CaBP, Mg-*Eh*CaBP, and holo-*Eh*CaBP by GdmCl was also monitored using CD at 222 nm (Figure 1C). Both thermal and chemical denaturation experiments with all the three forms of *Eh*CaBP were carried out by keeping the ionic strengths constant (90 mM NaCl in apo- and holo-*Eh*CaBP, 30 mM $MgCl_2$ in Mg-*Eh*CaBP) and the holo-*Eh*CaBP is saturated with Ca^{2+} by the addition of 5 mM $CaCl_2$ to the protein. The denaturant concentration at which half the protein is unfolded (C_M) is found to be 1.5, 1.9, and 5.6 M for apo-, Mg-bound, and holo-*Eh*CaBP, respectively. The free energy difference and the *m* values obtained by fitting the chemical denaturation curve to a two state model as discussed in Materials and Methods are shown in Figure 1D.

2D [^{15}N−^{1}H] HSQC of Mg-EhCaBP. Figure 2 shows 2D [^{15}N−^{1}H] HSQC of Mg-*Eh*CaBP. The number of peaks observed in the [^{15}N−^{1}H] HSQC of Mg-*Eh*CaBP is around 75, which is significantly less than the expected (134 residues). Further, the peaks are broad (*25*−*27*) due to line broadening effects because of the constrained conformational exchange that the protein undergoes in its Mg^{2+}-bound form in the μs to ms time scale (*28*, *29*). Moreover, variable intensities of peaks observed support the presence of several conformationally exchangeable species in the μs to ms time scale.

Earlier the [^{15}N−^{1}H] HSQC of apo-*Eh*CaBP has been shown to have a narrow dispersion in the backbone $^{1}H^{N}$ chemical shifts (7.20−8.75 ppm), and it accounted only for

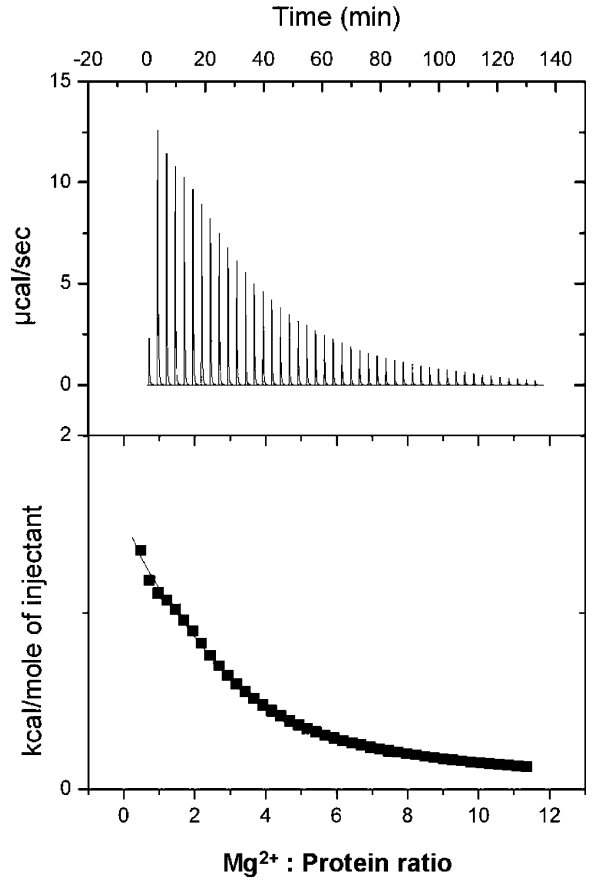

FIGURE 3: Calorimetric titration of 3 μL aliquots of 100 mM $MgCl_2$ solution into 850 μM Ca^{2+}-free *Eh*CaBP at 298 K. Plot of kcal/mol of heat absorbed/released per injection of $MgCl_2$ as a function of metal:protein ratio at 298 K is also shown. The best least-squares fit of the data to three site sequential binding model is given by the solid line.

one-third of the expected peaks (*17*). The HSQC of Mg-*Eh*CaBP on the other hand displays relatively sharper peaks (compared to that of the apo form) but significantly broader when compared with those of holo-*Eh*CaBP, and hence, no resonance assignments were possible. For comparison, [^{15}N−^{1}H] HSQC of all the three forms (apo-*Eh*CaBP, Mg-*Eh*CaBP, and holo-*Eh*CaBP) are shown in the Supporting Information (Figure S1). Expectedly, addition of Ca^{2+} in the presence or absence of Mg^{2+} transforms the protein into its holo form and the HSQC recorded with such a sample is identical to the one previously recorded with the holo-*Eh*CaBP. This suggests that *Eh*CaBP attains the same conformation after binding to Ca^{2+} both in the presence and in the absence of Mg^{2+}. This conclusion is also supported by the gel permeation chromatography and ANS binding studies.

EhCaBP has Three Mg^{2+} Binding Sites. Isothermal calorimetric titrations were carried out (at 298 K) to find out the number of Mg^{2+} binding sites in *Eh*CaBP. The ITC data suggests that Mg^{2+} binds to *Eh*CaBP very weakly in the millimolar range. Moreover, binding of Mg^{2+} to *Eh*CaBP is entropically driven (Figure 3). ITC data could be fitted to a sequential 3 site model, which is consistent with the NMR data discussed below. The thermodynamic parameters thus obtained are given in Table 1. The total free energy of Mg^{2+} binding thus obtained at 298 K is -11.5 ± 0.1 kcal mol^{-1}.

Ca^{2+} Titration of EhCaBP in the Presence of Mg^{2+}. To study the influence of Mg^{2+} on the equilibrium folding

Table 1: Summary of Macroscopic Binding Constants and Thermodynamic Parameters Obtained from the Mg^{2+} Binding Isotherm of *Eh*CaBP at 298 K

	macroscopic binding constants (M^{-1})	ΔH (kcal/mol)	$T\Delta S$ (kcal/mol)
K_1	1.4E3 ± 4E2	2.7 ± 0.1	6.9
K_2	1.5E3 ± 3E2	0.5 ± 0.1	4.9
K_3	1.4E2 ± 4	4.4 ± 0.1	7.3

pathway of *Eh*CaBP, from apo-*Eh*CaBP to holo-*Eh*CaBP, Ca^{2+} titration of apo-*Eh*CaBP was carried out in the presence of Mg^{2+}, and was compared with that in its absence by monitoring changes in the [$^{15}N-^{1}H$] HSQC. During the entire course of titration, no transient aggregation was observed as monitored using DLS experiments by similar titrations (data not shown), and the sample was found to be soluble and stable during the course of titration. At the end of the titration, the change in pH was less than 0.1 unit. During Ca^{2+} titration, several new peaks corresponding to the amide residues of the holo form started appearing in the HSQC, with a concomitant decrease in the intensity of of original peaks corresponding to the Mg-*Eh*CaBP. The transformation that the protein thus undergoes upon addition of Ca^{2+} is a slow exchange process in the NMR time scale.

The backbone $^{1}H^{N}$ of highly homologous Gly residues at the 6th position (Gly-6; G15, G51, G90, and G122) of the four Ca^{2+}-binding loops (Scheme 1) exhibit a characteristic downfield shift in the metal-bound form (holo) of the protein. Thus, the corresponding [$^{15}N-^{1}H^{N}$] peaks of these Gly-6 in the [$^{15}N-^{1}H$] HSQC appear in the least-crowded region and play the role of a hinge during the conformational switching from apo to holo forms (*9*). Hence, these [$^{15}N-^{1}H^{N}$] peaks act as good markers as described earlier (*17*).

The [$^{15}N-^{1}H$] HSQC of Mg-*Eh*CaBP (Figure 2) shows three [$^{15}N-^{1}H^{N}$] peaks in the region expected from the amide-pair [$^{15}N-^{1}H$] belonging to the Gly-6 residues, supporting that the Mg^{2+} binds to only three sites. These peaks gradually disappear upon Ca^{2+} titration with concomitant appearance of new cross peaks, which are representative of [Ca^{2+}]-bound state of the protein [Ca-*Eh*CaBP]. Figure 4A and Figure 4B show the plots of normalized [$^{15}N-^{1}H$] peak volumes corresponding to the three Gly-6 of Mg-*Eh*CaBP and four Gly-6 of Ca-*Eh*CaBP, respectively, as a function of metal (Ca^{2+}):protein ratio. As seen in Figure 4A, the three Gly-6 peaks of Mg-*Eh*CaBP disappear precisely at a stoichiometric metal (Ca^{2+}):protein ratio of 3.0, supporting the 3 site model described above for Mg^{2+} binding. On the other hand, as seen in Figure 4B, it is observed that G51 and G90 start appearing simultaneously around a metal: protein ratio of 1:1. This is followed with the appearance of G15 and G122, beyond a metal:protein ratio of 2:1 and 2.6: 1, respectively. To recall, in the absence of Mg^{2+} (*17*), first there was the gradual appearance of a cross peak belonging to only G51 (site II). Beyond the Ca^{2+}:protein ratio of 1.5: 1, G90, G15, and G122 started appearing almost together. This implies that, in the absence of Mg^{2+}, Ca^{2+} binds first to the N-terminal domain alone, specifically to site II. This is followed by sites III, I, and IV filling up almost together (*17*). In the presence of Mg^{2+}, sites in both domains, i.e., N-terminal (site II) and C-terminal (site III), bind to calcium simultaneously, suggesting a more cooperative folding of *Eh*CaBP toward its holo state.

It is clear from Figure 4B that the G122 of site IV is the last one to be filled by Ca^{2+}, after the Mg^{2+} displacement by Ca^{2+} from sites I, II, and III. Incidentally, it is the most specific site for Ca^{2+}.

Further, to establish that it is indeed sites I, II, and III that bind Mg^{2+}, titrations were carried out with the paramagnetic Mn^{2+} (*30*) as mentioned in Materials and Methods. Paramagnetic Mn^{2+} has an ionic radius of 0.74 Å, close to that of Mg^{2+}, and both these ions are known to prefer octahedral geometry with a coordination number 6 (*31*). When a small amount of Mn^{2+} was added to $[Ca^{2+}]_4$-*Eh*CaBP, in the presence Mg^{2+} it is observed that G51 broaden out first, followed by G15 and G90 (Figure 5). No observable changes were noticed in the case of G122 belonging to the fourth site. These observations taken together reveal that Mg^{2+} binds to the first three sites (namely, I, II, and III) out of four EF-hands present. The fourth site is known to be highly specific to Ca^{2+}.

Hydrogen Exchange of Backbone $^{1}H^{N}$ in Mg-EhCaBP. The [$^{1}H-^{2}H$] exchange of backbone $^{1}H^{N}$ for Mg-*Eh*CaBP has been monitored indirectly by transforming it into its holo form with a sudden addition of Ca^{2+} (*17*). In the presence of Mg^{2+}, deuterium exchange shows that all the [$^{15}N-^{1}H$] peaks disappear within a span of 2 h. To recall, in apo-*Eh*CaBP, all the peaks disappeared within 15 min at 25 °C (*17*). Residues protected at different time points are shown in Figure 6A. To quantify the [$^{1}H-^{2}H$] exchange rates (k_{ex}) of individual $^{1}H^{N}$ spins in Mg-*Eh*CaBP, we monitored their resonance decays, and the corresponding protection factors (PF) were measured. The $^{1}H^{N}$ PF values (Figure 6B) for Mg-*Eh*CaBP, though higher compared to those observed in apo-*Eh*CaBP, are found to be much smaller compared to holo-*Eh*CaBP (*17*). Further, unlike apo-*Eh*CaBP, both domains in Mg-*Eh*CaBP show comparable protection for individual $^{1}H^{N}$. Closer examination of Figure 6B reveals that the $^{1}H^{N}$ of residues belonging to the antiparallel β-sheets in both the domains are protected.

Energetics of Ca^{2+} Binding in Presence and Absence of Mg^{2+}. The intrinsic metal ion binding to proteins is entropically driven ($\Delta H > 0$) due to high dehydration enthalpy of divalent metal ions (*32*). However, owing to various thermodynamically coupled processes, the apparent metal ion binding can become enthalpy driven. One such thermodynamically coupled process is the conformational change that a protein might undergo on metal ion binding (*33*). Ca^{2+} sensor proteins are known to undergo huge conformational change upon Ca^{2+} binding, and hence the overall Ca^{2+} binding process should be enthalpy driven and can be explained as follows. The Ca^{2+} binding to a Ca^{2+} binding site is primarily a combination of Ca^{2+} desolvation (ΔH_{bind} and ΔS_{bind}) and conformational change (ΔH_{conf} and ΔS_{conf}) that the site has to undergo after binding to Ca^{2+}, and further the ΔH_{bind} can be approximated to zero (*16*, *33*). Hence, the ΔH measured from the Ca^{2+} binding to the protein site primarily correspond to the other thermodynamically coupled processes like conformational readjustment that the protein has to undergo on binding to Ca^{2+}. In the case of *Eh*CaBP the conformational changes that the protein undergoes on binding to Ca^{2+} leads to exposure of hydrophobic surface to the solvent (see below). Indeed, this is not an energetically favorable process. However, Ca^{2+} binding leads to gaining of free energy which can help the protein to overcome the

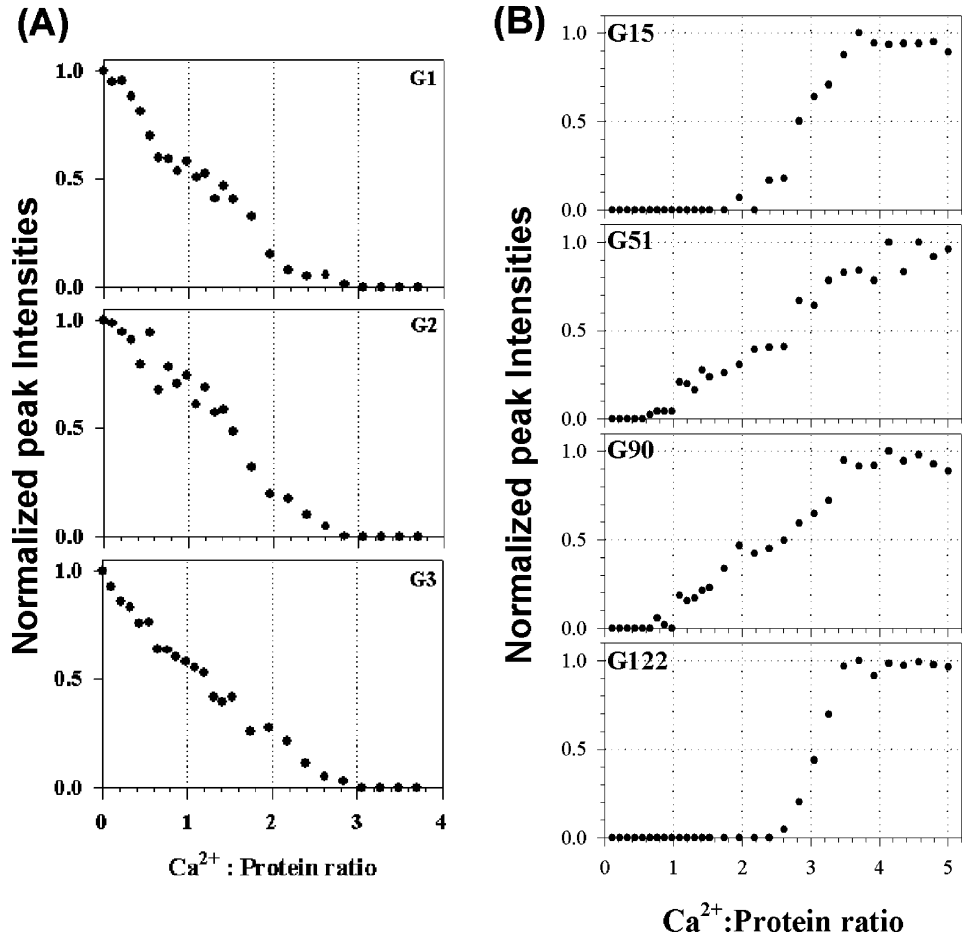

FIGURE 4: (A) Plots of normalized [^{15}N−^{1}H] peak volumes corresponding to the amino acid residues at G-6 of three calcium binding loops of Mg-*Eh*CaBP (see Figure 2), as a function of metal (Ca^{2+}):protein ratio. (B) Plots of normalized [^{15}N−^{1}H] peak volumes corresponding to the amino acid residues at G-6 (G15, G51, G90, and G122) of all the four Ca^{2+}-binding loops of Mg-*Eh*CaBP, as a function of metal (Ca^{2+}):protein ratio.

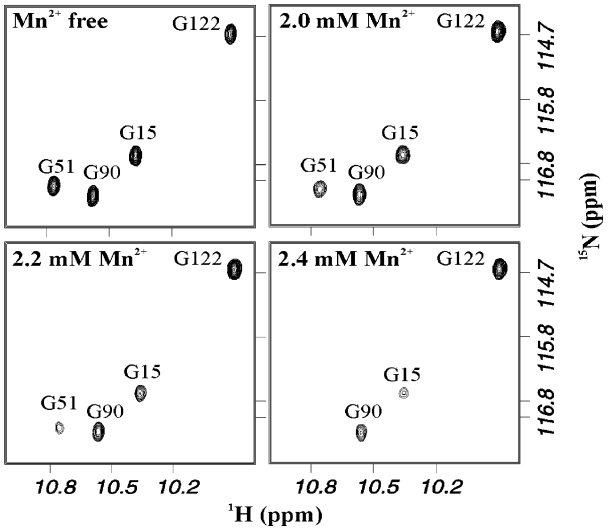

FIGURE 5: Selected region of 2D [^{15}N−^{1}H] HSQC recorded during the Mn^{2+} titration of *Eh*CaBP showing G15, G51, G90, and G122 peaks at different Mn^{2+} concentrations.

energy barrier of the energetically expensive conformational change. In the present case, this is experimentally observed by ITC (Figure 7). As seen in Figure 7, however, the Ca^{2+} binding isotherms in the absence and the presence of Mg^{2+} are significantly different. The data in both the cases could be fitted to 4 site sequential binding model with the lowest χ^2. The binding parameters thus obtained are given in Table 2.

In the absence of Mg^{2+}, the data reveals that three sites bind Ca^{2+} in an exothermic manner and one site in an endothermic manner. In the presence of Mg^{2+}, all the four sites exhibit exothermic process (Table 2) and the Ca^{2+} binding isotherm shows a distinct biphasic nature (Figure 7B). This could possibly be due to the combined effect of exothermic nature and weak Ca^{2+} binding affinity of the fourth Ca^{2+} binding site. In the absence of Mg^{2+} too, we notice that the fourth site is the weakest metal binding site, though this site still exhibits endothermic nature similar to the rest of the sites in the protein. The initial phase of Ca^{2+} binding in both the presence and the absence of Mg^{2+} is highly exothermic, indicating a high conformational change that the protein has to undergo upon initial Ca^{2+} binding. The exothermic nature in the initial phase is noticeably high in the presence of Mg^{2+} as compared to that in its absence. This might be due to higher degree of conformational change that the protein possibly might be undergoing in the presence of Mg^{2+} as compared to that in its absence. Based on thermal/chemical denaturation and nHX studies we notice that Mg^{2+}-*Eh*CaBP is more structured as compared to its apo form. Hence, it is possible that the Mg^{2+}-*Eh*CaBP has to undergo higher conformational change as compared to apo-*Eh*CaBP (*17*).

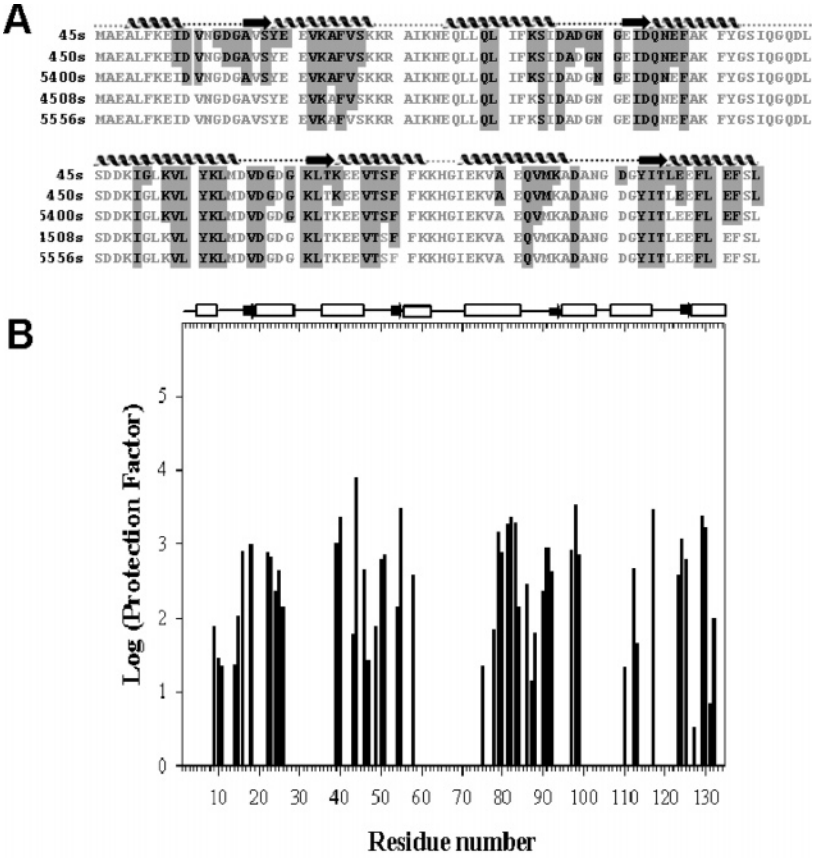

FIGURE 6: (A) Qualitative analysis of the ^2H_2O exchange experiment of Mg-*Eh*CaBP; the amino acid residues with intact $^1H^N$ are shown in black with a gray background, and those which exchanged fast are shown in gray. (B) Histogram showing the distribution of protection factors (PFs) from amide hydrogen exchange of Mg-*Eh*CaBP. The PFs are plotted on a logarithmic scale. The secondary structural elements are shown schematically above the plots.

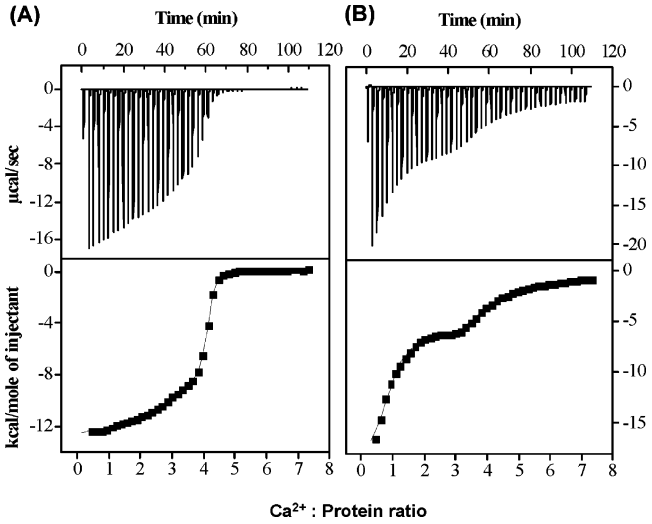

FIGURE 7: Calorimetric titration of 3 μL aliquots of 10 mM $CaCl_2$ solution into 0.145 mM Ca^{2+}-free *Eh*CaBP at 298 K (A) in the absence and (B) in the presence of Mg^{2+}. Plots of kcal/mol of heat absorbed/released per injection of $CaCl_2$ as a function of metal: protein ratio at 298 K in the absence and in the presence of Mg^{2+} are also shown. The best least-squares fit of the data to four site sequential binding model is given by the solid line.

The apparent total free energy of all the Ca^{2+} binding processes in both the presence and the absence of Mg^{2+} were calculated as follows:

$$\Delta G_{total} = -RT \ln(K_1K_2K_3K_4) \quad (5)$$

where K_1, K_2, K_3, and K_4 are the ITC derived macroscopic binding constants (*34*). The ΔG_{total} of Ca^{2+} binding thus obtained at 298 K in the presence and absence of Mg^{2+} are -28.9 ± 0.1 and -30.0 ± 0.1 kcal mol^{-1} respectively. Although the ΔG_{total} measured in the presence and absence of Mg^{2+} are almost similar, it is worthwhile to note that in the presence of Mg^{2+} a free energy of 11.5 ± 0.1 kcal mol^{-1} has been spent by the system to displace the bound Mg^{2+}.

Ca^{2+} Binding to EhCaBP Is More Cooperative in the Presence of Mg^{2+}. ANS fluorescence is strongly dependent on the local environment. As seen in Figure 8A, the emission of ANS is weak in water with a maximum at 515 nm. Apo-*Eh*CaBP, Mg-*Eh*CaBP, and holo-*Eh*CaBP bind to ANS and result in significant enhancement in the fluorescence associated with large blue shifts of 39, 32, and 43 nm, respectively. This data suggests significant exposure of hydrophobic pockets in apo-*Eh*CaBP, which is about 4-fold smaller compared to those in holo-*Eh*CaBP. Interestingly, the ANS fluorescence for apo-*Eh*CaBP is around 1.5-fold higher compared to that of Mg-*Eh*CaBP. This data establishes that Mg-*Eh*CaBP adopts relatively more *closed conformation* (i.e., buried hydrophobic patches) compared to that in its apo form. These observations taken together reveal that the binding of Mg^{2+} stabilizes the *closed conformation* of the Ca^{2+}-free form of *Eh*CaBP.

Figure 8B shows Ca^{2+} titration of apo-*Eh*CaBP in the presence and the absence of Mg^{2+}. The raw data corresponding to these titrations are shown in the Supporting Information (Figure 2S). It is evident from Figure 8B that the Ca^{2+}-

Table 2: Summary of Macroscopic Binding Constants and Thermodynamic Parameters Obtained from the Ca^{2+} Binding Isotherm of *Eh*CaBP in the Absence and in the Presence of Mg^{2+} at 298 K

	macroscopic binding constants (M^{-1})		ΔH (kcal/mol)		$T\Delta S$ (kcal/mol)	
	absence of Mg^{2+}	presence of Mg^{2+}	absence of Mg^{2+}	presence of Mg^{2+}	absence of Mg^{2+}	presence of Mg^{2+}
K_1	7.5E4 ± 1E3	1.8E6 ± 4E4	−11.2 ± 0.8	−19.9 ± 1.1	−4.5	−11.4
K_2	4E6 ± 6E4	2.4E5 ± 1E4	−13.8 ± 0.5	−15.4 ± 0.6	−4.8	5.8
K_3	1.2E4 ± 3E2	7.5E5 ± 3E4	−35.0 ± 1.3	−8.5 ± 0.1	−29.4	−0.5
K_4	2.8E6 ± 6E4	5.1E3 ± 2E2	16.2 ± 1.2	−14.5 ± 0.2	24.9	−9.4

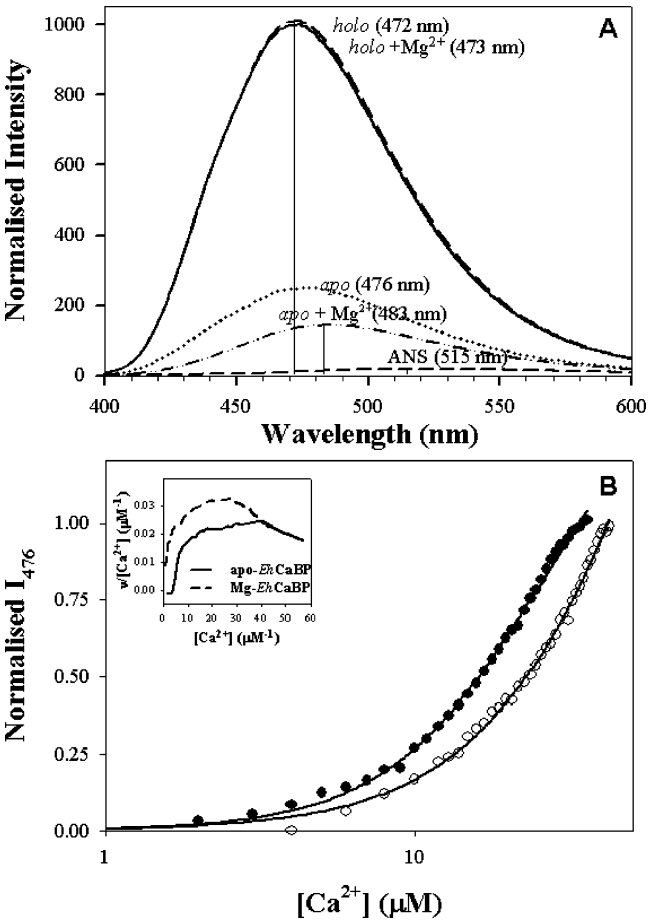

FIGURE 8: (A) ANS fluorescence emission spectra of apo-*Eh*CaBP, Mg-*Eh*CaBP, and holo-*Eh*CaBP with excitation at 389 nm. (B) Ca^{2+}-induced conformational change in ANS fluorescence emission during Ca^{2+} titration of ANS saturated apo-*Eh*CaBP (open circle) and Mg-*Eh*CaBP (filled circle), measured at 472 nm with excitation at 389 nm. The Hill equation (solid line) was fitted to a semilogarithmic plot of the normalized intensity. Positive cooperativity between sites is shown in the inset by the upward curved Scatchard plot; ν is the fraction of total number of sites that are bound.

free form of the protein responds to noticeably lower concentration of Ca^{2+} in the presence of Mg^{2+} than in its absence. This suggests a higher cooperativity for exposure of hydrophobic core due to Ca^{2+} binding in the presence of Mg^{2+}. We calculated the Hill coefficients for the Ca^{2+} titration both in the presence and in the absence of Mg^{2+}. Hill coefficients for apo-*Eh*CaBP (1.44 ± 0.07) and Mg-*Eh*CaBP (1.68 ± 0.06) suggest that the conformational changes on binding to Ca^{2+} are positively cooperative in both forms. This was shown by the upward curvature of the Scatchard plot (Figure 8B, inset). The more curved nature of the Scatchard plot seen in the presence of Mg^{2+} indicates higher cooperativity of conformational change upon binding to Ca^{2+} (Figure 8B inset). It is worthwhile to note that the window of Ca^{2+} concentration in which *Eh*CaBP responds and undergoes conformational change required for its functioning is smaller in the presence of Mg^{2+} than in its absence. This is very important for the functioning of *Eh*CaBP as a signaling protein. Moreover, the extent of hydrophobic patch exposed on binding to Ca^{2+} remains the same in the presence and the absence of Mg^{2+} as the intensity of fluorescence signal due to ANS binding in both cases superimposes (Figure 8A) suggesting that the holo *Eh*CaBP has identical structure both in the presence and in the absence of Mg^{2+}.

DISCUSSION

Stability and Structural Integrity of Mg-EhCaBP. Apo-*Eh*CaBP binds Mg^{2+} and exists in a monomeric form. Mg-*Eh*CaBP is found to possess a globular volume which is intermediate between that of apo and holo forms. Unlike the holo-*Eh*CaBP, Mg-*Eh*CaBP is highly sensitive to temperature and GdmCl concentrations. However, it is comparatively more stable than the apo-*Eh*CaBP. This reveals that Mg^{2+} imparts a significant amount of stability to apo-*Eh*CaBP against thermal as well as chemical denaturation. Moreover, it is apparent from the denaturation studies that unfolding of Mg-*Eh*CaBP is more cooperative than apo-*Eh*CaBP as revealed by the sharp transition observed in both thermal and chemical denaturation data (Figure 1B and 1C). From Figure 1D it is evident that the holo form has the highest energy of unfolding (ΔG_{uf}) followed by Mg-*Eh*CaBP, which in turn is followed by the apo form suggesting that Mg-*Eh*CaBP has intermediate stability compared to that of holo and apo forms of *Eh*CaBP. The *m* value, which is the measure of the dependence of the protein stability on the denaturant concentration, of the three forms in the increasing order is given as

Mg-*Eh*CaBP > apo-*Eh*CaBP > holo-*Eh*CaBP

The [GdmCl] dependence or the *m* value for Mg-*Eh*CaBP is the highest indicating a more cooperative nature of unfolding for Mg-*Eh*CaBP as compared to both the other forms. This is also evident from the sigmoidal nature of the chemical denaturation curve (Figure 1C) which is steepest in the case of Mg-*Eh*CaBP. In fact, in the thermal unfolding study (Figure 1B) too, we have observed a similar type of behavior, i.e., a sigmoid-like sudden increase in the unfolding beyond 80 °C, which was not in the case of the apo form. Hence both the denaturation studies establish that the Mg-*Eh*CaBP unfolds in a cooperative manner. In fact the thermal and denaturation profiles of *Nereis* Sarcoplasmin calcium binding protein (NSCP), a calcium buffer reported earlier (*24*) in its apo, Mg-bound, and holo forms suggested a similar

type of stability and cooperativity as reported here in the case of *Eh*CaBP.

The stability and structural integrity of Mg-*Eh*CaBP is reflected in the observed PFs in Mg-*Eh*CaBP (Figure 5B), which are higher compared to those observed in apo-*Eh*CaBP. Both domains have similar PFs in Mg-*Eh*CaBP (Figure 5B) unlike those observed in apo-*Eh*CaBP, wherein the C-terminal domain is found to be more protected than the N-terminal counterpart (*17*). However, absolute values of PFs are substantially smaller compared to the corresponding values observed in holo-*Eh*CaBP. This hints at the weakening of hydrogen bonds and/or hydrophobic interactions in Mg-*Eh*CaBP compared to holo-*Eh*CaBP. However, HX studies reveal that Mg^{2+}-binding to both the EF-hands in the N-terminal domain imparts a considerable amount of protection to the backbone $^1H^N$ present therein. This results in increased structural stability of the protein in Mg^{2+}-bound form. Surprisingly, the IV EF-hand which does not bind Mg^{2+} attains comparable protection, due to the stabilization of the tertiary fold of C-terminal domain via antiparallel β-sheet formation as site-III bind Mg^{2+} (*35*).

Further, the observed cooperativity in chemical and thermal denaturation studies can be attributed to the intradomain cooperativity due to the stabilization of the antiparallel β-sheets in both the domains. In this context, we cannot rule out the interdomain cooperativity as the Ca^{2+} titration in the absence and the presence of Mg^{2+} monitored by NMR and ITC reveal a large difference in the Ca^{2+} binding pattern. Thus Mg^{2+} not only imparts stability to the Ca^{2+}-free form of *Eh*CaBP but also provides structural integrity to it thereby making the protein a structurally cooperative unit.

Mg^{2+} Stabilizes the Closed Conformation of Apo-EhCaBP. *Eh*CaBP undergoes a huge conformational change and thus exposes its hydrophobic patches upon addition of Ca^{2+}. This is a property demonstrated by calcium sensors. In its apo state though *Eh*CaBP exposes hydrophobic patche(s), the amount of exposure is significantly smaller compared with that of the holo form. However, the exposure observed in the apo state has been attributed earlier due to the partially unfolded nature of the protein in this state (*17*). Thus, the apo form has a more *closed conformation* as expected for a Ca^{2+} sensor and in the holo form it adopts an *open conformation* with the exposure of hydrophobic patches. Addition of Mg^{2+} to the apo state further diminishes the ANS fluorescence (Figure 8A), a consequence of the further burial of the hydrophobic core thereby suggesting that the Mg^{2+} binding stabilizes the *closed conformation* of *Eh*CaBP. This is similar to many EF-hands in CaBPs that have the ability to bind Mg^{2+} apart from Ca^{2+}, though with lower affinity (*13*, *14*, *36*−*38*). For example, in calbindin D_{9k}, a Ca^{2+} buffer protein, Mg^{2+} binding to the regular EF-hand leads to decrease in interhelical angle between helix III and IV to a more compact form as compared to both the Ca^{2+} loaded and metal ion-free forms (*39*). This was attributed to the smaller ionic size of Mg^{2+} where six-coordination geometry is preferred. In fact, even the $(Mg^{2+})_1(Ca^{2+})_1$ state of the N-terminal domain of CaM has a conformation more similar to the *closed conformation* observed in apo and $(Mg^{2+})_2$ states than to the open $(Ca^{2+})_2$ state (*40*). This indicates that the *Eh*CaBP in Ca^{2+}-free form adopts a *closed conformation* without the exposure of the hydrophobic core as observed in the apo form of CaM (*41*).

The mechanism of stabilization of the *closed conformation* can be explained satisfactorily by the recently proposed EF-hand β-scaffold model (EFBS model) which explains the mechanism of Ca^{2+} binding to the EF-hand (*42*). According to this model, Ca^{2+} binds initially to the N-terminal stretch of the EF-loop, establishing a rigid link between the E-helix and the EFβ-scaffold, which comprises the bond network involving the carbonyl oxygen of the +7 residue (+Y position, see Scheme 1) in the EF-loop and the two hydrogen bonds of the +8 residue (a hydrophobic residue and which is a part of the small antiparallel β-strand). Next, the backbone torsional flexibility in the EFβ-scaffold enables the F-helix to change its orientation so that the bidentate Glu ligand in the +12th position can move into appropriate Ca^{2+} coordinating position. In this model, the variable N-terminal stretch of the EF-loop immobilizes the Ca^{2+} and positions it for the interaction with the last ligand, while the precise movement of the C-terminal strech drives the conformational change.

On the other hand, Mg^{2+} strongly prefers six coordination geometry, where the bidentate Glu ligand in the +12 position of the EF-hand becomes monodentate. Thus from the above, it can be said that Mg^{2+} first binds to the N-terminal stretch of the EF-loop establishing a rigid link with the EFβ-scaffold and then the F-helix which changes its orientation to accommodate the bidentate Glu in +12th position in the case of Ca^{2+}, now no longer undergoes conformational change since Mg^{2+} need not accommodate the bidentate Glu (+12) in its required six coordination geometry. Thus, binding of Mg^{2+} retains the *closed conformation* of the EF-hand in the apo state. In the case of *Eh*CaBP this conformation is further stabilized because of structurally more ordered form of Mg-*Eh*CaBP than its apo form.

Understanding the Differences in the Energetics of Mg^{+2} and Ca^{2+} Binding Processes. Ca^{2+} binding to an EF-hand is an energetically complex process. The free energy of Ca^{2+} binding to an EF-hand (ΔG) can be represented by the following equation of ligand interaction (*43*):

$$\Delta G = \Delta G_{t+r} + \sum \Delta G_r + (A)(\Delta G_h) + \Sigma \Delta G_{hb} + \sum \Delta G_{ionic} + n\Delta G_{hyd} \quad (6)$$

where ΔG_{t+r} and $\sum \Delta G_r$ are the free energy cost of restricting the overall motion and the internal rotation of the ligand and the EF-hand that is restrained upon binding, respectively. Both these terms are adverse entropy terms which oppose ligand-binding. On the other hand, ΔG_h is the free energy benefit due to the removal of 1 Å^2 of hydrocarbon surface area from water upon binding, which is the result of hydrophobic effect. It is multiplied by the buried surface area (A) for each specified case. ΔG_{hb} and ΔG_{ionic} are the free energy benefit of a hydrogen bond and an ionic bond in the binding site summed over all such hydrogen and ionic bonds, respectively. ΔG_{hyd} is the free energy of desolvation of the ligand, and n is the number of molecules of water of hydration. This is an additional term introduced to the equation mentioned in ref 43.

In the case of Ca^{2+} and Mg^{2+} binding to the apo protein the first two terms are adverse entropy terms and oppose ligand binding. But the expenditure of energy during Ca^{2+} binding for internal motions ($\Delta G_{t+r} + \sum \Delta G_r$) is compara-

tively less in the presence of Mg^{2+} as the system is already in a restricted motion compared to apo. The ΔG_{hb} and ΔG_{ionic} terms are favorable in all the metal binding events. ΔG_{hyd} is favorable in all the cases of metal binding to a varying extent. ΔG_{hyd} depends on the number of H_2O molecules released in the binding process thereby leading to favorable entropy. The benefit of ΔG_{hyd} is highest for four Ca^{2+} binding to apo-*Eh*CaBP followed by three Mg^{2+} binding to apo-*Eh*CaBP and then by four Ca^{2+} binding to Mg-*Eh*CaBP where Mg^{2+} ions have to be solvated after displacement. The ΔG_h term is favorable for Mg^{2+} binding since addition of Mg^{2+} leads to burial of the hydrophobic core further compared to apo. In the case of Ca^{2+} binding both in the presence and in the absence of Mg^{2+}, exposure of hydrophobic core occurs. Therefore ΔG_h is unfavorable. Further it is comparatively more unfavorable in the presence of Mg^{+2} as it has to open more hydrophobic core than in the case of apo. Indeed this complex behavior of various free energy terms is responsible for the observed differences in the Ca^{2+} binding properties in *Eh*CaBP in the presence and in the absence of Mg^{2+} monitored by various biophysical experiments that include NMR. Further it is evident from our experimental results that these differences in binding properties in the presence of Mg^{2+} lead to a finer tuning of the range of Ca^{2+} concentration required for its conformational switching action in a more cooperative manner which is essential to carry out the signal transduction processes in a more efficient manner.

BIOLOGICAL RELEVANCE

Recently a number of EF-hand CaBPs have been reported to show their collapsed nature in metal-free forms (*16*−*18*, *44*−*46*). Understanding the functional role of such proteins is an important aspect of current structural biology. *Eh*CaBP is one among such EF-CaBPs, which has partially collapsed structure in its Ca^{2+}-free form. However, this form is significantly stabilized by Mg^{2+} which is abundant in the cell cytoplasm suggesting a possibility that *Eh*CaBP is Mg^{2+} bound in the resting cell. An important phenomenon observed here is the binding of Mg^{2+} that enhances the structural integrity of *Eh*CaBP, which in turn results in conformational switching upon addition of Ca^{+2} with positive cooperativity. Thus, the presence of Mg^{2+} leads to a fine-tuning of the Ca^{2+} concentration required for the protein to switch its conformation from a *closed* state to an *open* state in order to carry out various signal transduction processes.

ACKNOWLEDGMENT

We thank Prof. Alok Bhattacharya (JNU, New Delhi) for providing the *Eh*CaBP clone, and Prof. Walter Chazin (Vanderbilt University, USA) and Prof. Girjesh Govil (TIFR) for their critical comments.

SUPPORTING INFORMATION AVAILABLE

2D [$^{15}N-^{1}H$] HSQC spectra (Figure 1S) and raw plots of Ca^{2+}-induced conformational changes in ANS fluorescence emission during Ca^{2+} titration (Figure 2S). This material is available free of charge via the Internet at http://pubs.acs.org.

REFERENCES

1. Ikura, M. (1996) Calcium binding and conformational response in EF-hand proteins, *Trends Biochem. Sci. 21*, 14−17.
2. Kretsinger, R. H., and Nockolds, C. E. (1973) Carp muscle calcium-binding protein. II. Structure determination and general description, *J. Biol. Chem. 248*, 3313−3326.
3. Nelson, M. R., and Chazin, W. J. (1998) Structures of EF-hand Ca(2+)-binding proteins: diversity in the organization, packing and response to Ca2+ binding, *Biometals 11*, 297−318.
4. Strynadka, N. C., and James, M. N. (1989) Crystal structures of the helix-loop-helix calcium-binding proteins, *Annu. Rev. Biochem. 58*, 951−998.
5. Wang, Z., Gergely, J., and Tao, T. (1992) Characterization of the Ca(2+)-triggered conformational transition in troponin C, *Proc. Natl. Acad. Sci. U.S.A. 89*, 11814−11817.
6. Trave, G., Lacombe, P. J., Pfuhl, M., Saraste, M., and Pastore, A. (1995) Molecular mechanism of the calcium-induced conformational change in the spectrin EF-hands, *EMBO J. 14*, 4922−4931.
7. Zhang, M., Tanaka, T., and Ikura, M. (1995) Calcium-induced conformational transition revealed by the solution structure of apo calmodulin, *Nat. Struct. Biol. 2*, 758−767.
8. Houdusse, A., Love, M. L., Dominguez, R., Grabarek, Z., and Cohen, C. (1997) Structures of four Ca2+-bound troponin C at 2.0 A resolution: further insights into the Ca2+-switch in the calmodulin superfamily, *Structure 5*, 1695−1711.
9. Falke, J. J., Drake, S. K., Hazard, A. L., and Peersen, O. B. (1994) Molecular tuning of ion binding to calcium signaling proteins, *Q. Rev. Biophys. 27*, 219−290.
10. Cates, M. S., Teodoro, M. L., and Phillips, G. N., Jr. (2002) Molecular mechanisms of calcium and magnesium binding to parvalbumin, *Biophys. J. 82*, 1133−1146.
11. Linse, S., and Forsen, S. (1995) Calcium Regulation of Cellular Function (Means, A. R., Ed.) pp 89−152, Raven Press, New York.
12. da Silva, A. C., Kendrick-Jones, J., and Reinach, F. C. (1995) Determinants of ion specificity on EF-hands sites. Conversion of the Ca2+/Mg2+ site of smooth muscle myosin regulatory light chain into a Ca(2+)-specific site, *J. Biol. Chem. 270*, 6773−6778.
13. Ohki, S., Ikura, M., and Zhang, M. (1997) Identification of Mg2+-binding sites and the role of Mg2+ on target recognition by calmodulin, *Biochemistry 36*, 4309−4316.
14. Wingard, J. N., Chan, J., Bosanac, I., Haeseleer, F., Palczewski, K., Ikura, M., and Ames, J. B. (2005) Structural analysis of Mg2+ and Ca2+ binding to CaBP1, a neuron-specific regulator of calcium channels, *J. Biol. Chem. 280*, 37461−37470.
15. Berggard, T., Miron, S., Onnerfjord, P., Thulin, E., Akerfeldt, K. S., Enghild, J. J., Akke, M., and Linse, S. (2002) Calbindin D28k exhibits properties characteristic of a Ca2+ sensor, *J. Biol. Chem. 277*, 16662−16672.
16. Yamniuk, A. P., Nguyen, L. T., Hoang, T. T., and Vogel, H. J. (2004) Metal ion binding properties and conformational states of calcium- and integrin-binding protein, *Biochemistry 43*, 2558−2568.
17. Mukherjee, S., Kuchroo, K., and Chary, K. V. (2005) Structural characterization of the apo form of a calcium binding protein from Entamoeba histolytica by hydrogen exchange and its folding to the holo state, *Biochemistry 44*, 11636−11645.
18. Gombos, Z., Durussel, I., Ikura, M., Rose, D. R., Cox, J. A., and Chakrabartty, A. (2003) Conformational coupling of Mg2+ and Ca2+ on the three-state folding of calexcitin B, *Biochemistry 42*, 5531−5539.
19. Atreya, H. S., Sahu, S. C., Bhattacharya, A., Chary, K. V., and Govil, G. (2001) NMR derived solution structure of an EF-hand calcium-binding protein from Entamoeba Histolytica, *Biochemistry 40*, 14392−14403.
20. Sahu, S. C., Bhattacharya, A., Chary, K. V., and Govil, G. (1999) Secondary structure of a calcium binding protein (CaBP) from Entamoeba histolytica, *FEBS Lett. 459*, 51−56.
21. Santoro, M. M., and Bolen, D. W. (1988) Unfolding free energy changes determined by the linear extrapolation method. 1. Unfolding of phenylmethanesulfonyl alpha-chymotrypsin using different denaturants, *Biochemistry 27*, 8063−8068.
22. Wiseman, T., Williston, S., Brandts, J. F., and Lin, L. N. (1989) Rapid measurement of binding constants and heats of binding using a new titration calorimeter, *Anal. Biochem. 179*, 131−137.
23. Kay, L. E., Keifer, P., and Saarinen, T. (1992) Pure absorption gradient enhanced heteronuclear single quantum correlation spectroscopy with improved sensitivity, *J. Am. Chem. Soc. 114*, 10663−10665.
24. Christova, P., Cox, J. A., and Craescu, C. T. (2000) Ion-induced conformational and stability changes in Nereis sarcoplasmic calcium binding protein: evidence that the APO state is a molten globule, *Proteins 40*, 177−184.

25. Rao, B. D. (1989) Nuclear magnetic resonance line-shape analysis and determination of exchange rates, *Methods Enzymol. 176*, 279−311.
26. Linse, S., and Chazin, W. J. (1995) Quantitative measurements of the cooperativity in an EF-hand protein with sequential calcium binding, *Protein Sci. 4*, 1038−1044.
27. Mohan, P. M., Barve, M., Chatterjee, A., and Hosur, R. V. (2006) pH driven conformational dynamics and dimer-to-monomer transition in DLC8, *Protein Sci. 15*, 335−342.
28. Baum, J., Dobson, C. M., Evans, P. A., and Hanley, C. (1989) Characterization of a partly folded protein by NMR methods: studies on the molten globule state of guinea pig alpha-lactalbumin, *Biochemistry 28*, 7−13.
29. Schulman, B. A., Kim, P. S., Dobson, C. M., and Redfield, C. (1997) A residue-specific NMR view of the non-cooperative unfolding of a molten globule, *Nat. Struct. Biol. 4*, 630−634.
30. Zuleeg, T., Hartmann, R. K., Kreutzer, R., and Limmer, S. (2001) NMR spectroscopic evidence for Mn(2+)(Mg(2+)) binding to a precursor-tRNA microhelix near the potential RNase P cleavage site, *J. Mol. Biol. 305*, 181−189.
31. Bock, C. W., Katz, A. K., Markham, G. D., and Glusker, J. P. (1999) Manganese as a Replacement for Magnesium and Zinc: Functional Comparison of the Divalent Ions, *J. Am. Chem. Soc. 121*, 7360−7372.
32. Henzl, M. T., Larson, J. D., and Agah, S. (2003) Estimation of parvalbumin Ca(2+)- and Mg(2+)-binding constants by global least-squares analysis of isothermal titration calorimetry data, *Anal. Biochem. 319*, 216−233.
33. Gilli, R., Lafitte, D., Lopez, C., Kilhoffer, M., Makarov, A., Briand, C., and Haiech, J. (1998) Thermodynamic analysis of calcium and magnesium binding to calmodulin, *Biochemistry 37*, 5450−5456.
34. Linse, S., Helmersson, A., and Forsen, S. (1991) Calcium binding to calmodulin and its globular domains, *J. Biol. Chem. 266*, 8050−8054.
35. Shaw, G. S., Hodges, R. S., and Sykes, B. D. (1990) Calcium-induced peptide association to form an intact protein domain: 1H NMR structural evidence, *Science 249*, 280−283.
36. Malmendal, A., Evenas, J., Thulin, E., Gippert, G. P., Drakenberg, T., and Forsen, S. (1998) When size is important. Accommodation of magnesium in a calcium binding regulatory domain, *J. Biol. Chem. 273*, 28994−29001.
37. Martin, S. R., Lu, A. Q., Xiao, J., Kleinjung, J., Beckingham, K., and Bayley, P. M. (1999) Conformational and metal-binding properties of androcam, a testis-specific, calmodulin-related protein from Drosophila, *Protein Sci. 8*, 2444−2454.
38. Finley, N. L., Howarth, J. W., and Rosevear, P. R. (2004) Structure of the Mg2+-loaded C-lobe of cardiac troponin C bound to the N-domain of cardiac troponin I: comparison with the Ca2+-loaded structure, *Biochemistry 43*, 11371−11379.
39. Andersson, M., Malmendal, A., Linse, S., Ivarsson, I., Forsen, S., and Svensson, L. A. (1997) Structural basis for the negative allostery between Ca(2+)- and Mg(2+)-binding in the intracellular Ca(2+)-receptor calbindin D9k, *Protein Sci. 6*, 1139−1147.
40. Malmendal, A., Linse, S., Evenas, J., Forsen, S., and Drakenberg, T. (1999) Battle for the EF-hands: magnesium-calcium interference in calmodulin, *Biochemistry 38*, 11844−11850.
41. Kuboniwa, H., Tjandra, N., Grzesiek, S., Ren, H., Klee, C. B., and Bax, A. (1995) Solution structure of calcium-free calmodulin, *Nat. Struct. Biol. 2*, 768−776.
42. Grabarek, Z. (2006) Structural basis for diversity of the EF-hand calcium-binding proteins, *J. Mol. Biol. 359*, 509−525.
43. Williams, D. H., Stephens, E., Zhou, M., and Zerella, R. (2004) Contributions to the catalytic efficiency of enzymes, and the binding of ligands to receptors, from improvements in packing within enzymes and receptors, *Methods Enzymol. 380*, 3−19.
44. Precheur, B., Cox, J. A., Petrova, T., Mispelter, J., and Craescu, C. T. (1996) Nereis sarcoplasmic Ca2+-binding protein has a highly unstructured apo state which is switched to the native state upon binding of the first Ca2+ ion, *FEBS Lett. 395*, 89−94.
45. Lytle, B. L., Volkman, B. F., Westler, W. M., and Wu, J. H. (2000) Secondary structure and calcium-induced folding of the Clostridium thermocellum dockerin domain determined by NMR spectroscopy, *Arch. Biochem. Biophys. 379*, 237−244.
46. Jeromin, A., Muralidhar, D., Parameswaran, M. N., Roder, J., Fairwell, T., Scarlata, S., Dowal, L., Mustafi, S. M., Chary, K. V., and Sharma, Y. (2004) N-terminal myristoylation regulates calcium-induced conformational changes in neuronal calcium sensor-1, *J. Biol. Chem. 279*, 27158−27167.

BI0621260